

Layer-by-layer stacked amorphous V₂O₅/Graphene 2D heterostructures with strong-coupling effect for high-capacity aqueous zinc-ion batteries with ultra-long cycle life

Xiao Wang ^{a,b,1}, Yaguang Li ^{a,1}, Pratteek Das ^{a,b}, Shuanghao Zheng ^a, Feng Zhou ^a, Zhong-Shuai Wu ^{a,*}

^a Dalian National Laboratory for Clean Energy, Dalian Institute of Chemical Physics, Chinese Academy of Sciences, 457 Zhongshan Road, Dalian, 116023, PR China

^b University of Chinese Academy of Sciences, 19 A Yuquan Road, Shijingshan District, Beijing, 100049, PR China



ARTICLE INFO

Keywords:

Zinc ion batteries
2D heterostructures
Ultra-long cycle life
V₂O₅/Graphene
Micro-batteries

ABSTRACT

The aqueous zinc-ion batteries (ZIBs) are highly competitive, exceptionally safe electrochemical energy storage devices, but suffer from the poor cyclability and unattainable capacity caused by structural instability of cathode materials. In this work, we reported a general 2D template ion-adsorption approach to assemble 2D amorphous V₂O₅/graphene heterostructures with highly stable layer-by-layer stacked structure and ultrathin thickness of 6 nm, for high-safe, rechargeable aqueous ZIBs. Owing to the unique features with strong synergistic effect, the resulting ZIBs show high capacity of 447 mAh/g at 0.3 A/g, extraordinary rate capability of 202 mAh/g at 30 A/g, and ultra-long lifespan up to 20,000 cycles at 30 A/g, greatly outperforming the vanadium based ZIBs reported. Moreover, the new-concept planar interdigital zinc ion micro-batteries, constructed by mask-assisted filtration strategy, display large volumetric capacity of 63 mAh/cm³ at 0.2 mA/cm², high volumetric energy density of 49 mWh/cm³, robust flexibility, and impressive modular integration in series and in parallel for boosting the capacity and voltage output, demonstrative of great potential as microscale power sources. Therefore, this approach will offer various opportunities to construct layer-by-layer stacked 2D heterostructures with fast ion-electron conductivity for ZIBs and other batteries.

1. Introduction

Lithium ion batteries are currently the major power sources for electric vehicles and portable electronics [1,2], but large-scale applications of lithium ion batteries in the future might be substantially hindered by the safety issue and limited lithium resource [3–5]. To overcome this, aqueous rechargeable nonlithium metal ion batteries, including monovalent (e.g., Na⁺ and K⁺) [6,7] and multivalent (e.g., Zn²⁺, Al³⁺ and Mg²⁺) [8], have been extensively developed as promising alternatives especially for grid-scale energy storage applications, due to the environmental benignity, abundant sources, and higher ionic conductivity of >10⁻¹ S/cm than organic electrolyte (~10⁻³ S/cm) [9]. Among them, aqueous zinc-ion batteries (ZIBs) hold the merits of earth abundance of Zn sources, high theoretical capacity (820 mAh/g), low redox potential (−0.76 V vs. SHE), and extraordinary water compatibility of Zn in comparison with alkaline metals [10]. However, the ZIBs are presently facing huge scientific

challenges lacking of the highly structure-stable cathodes associated with high capacity and long cycle life [11].

Great efforts for addressing these problems have been devoted to exploiting advanced cathode materials for ZIBs, including manganese oxides [12–14], Prussian blue analogues (e.g., FeFe(CN)₆) [15], NASICON-typed materials (e.g., Na₃V₂(PO₄)₃) [16], vanadium-based compounds (e.g., V₂O₅·nH₂O [10], VOPO₄ [17], Na_{0.33}V₂O₅ [18], Li_x·V₂O₅·nH₂O [19], NaCa_{0.6}V₆O₁₆·3H₂O [20], Zn_{0.3}V₂O₅·1.5H₂O [21], Na_{1.1}V₃O_{7.9} [22], VO₂ [23]), and organic compounds (e.g., pyrene-4,5,9,10-tetraone [24], polyaniline [25]). Special emphasis is given to high-capacity crystalline vanadium oxides for aqueous ZIBs [9] featured with low-cost and easy production, but they show poor sustainability caused by elements dissolution, self-aggregation, low conductivity, and active materials phase change derived from Zn²⁺ uptake and removal [26–28]. From this perspective, one reliable strategy for constructing high-performance ZIBs is to manufacture 2D graphene-based

* Corresponding author.

E-mail address: wuzs@dicp.ac.cn (Z.-S. Wu).

¹ These authors contributed equally.

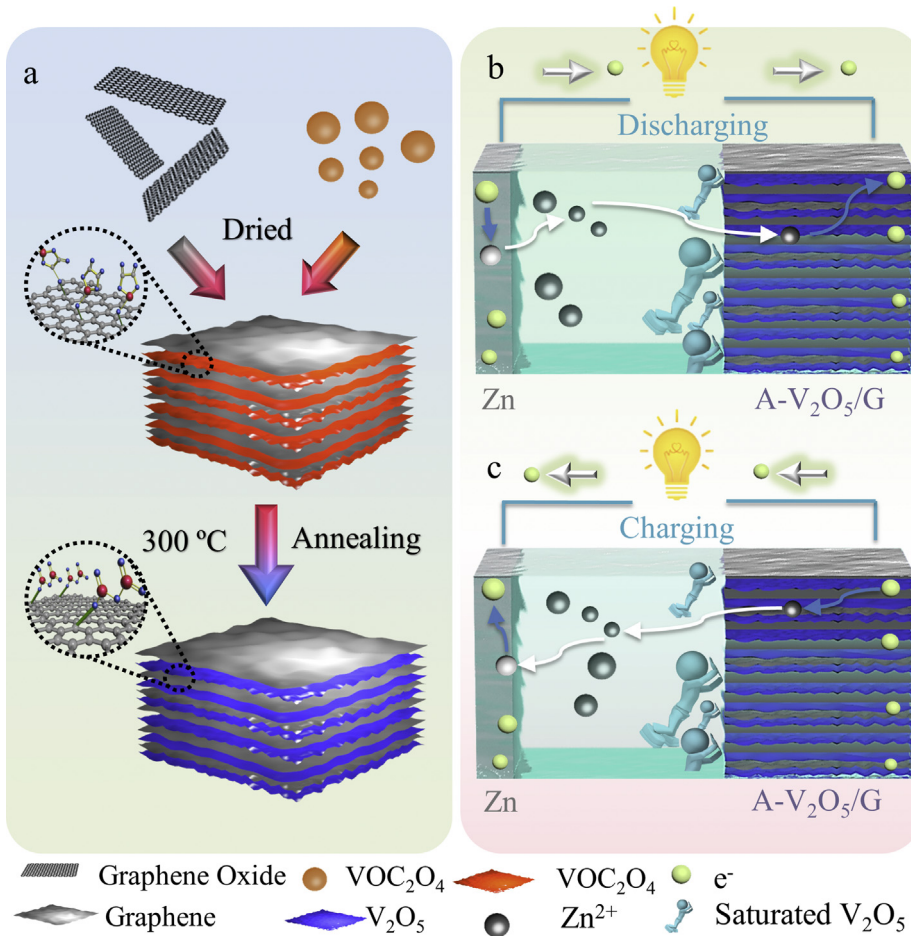


Fig. 1. Schematic illustration of the fabrication process of 2D A-V₂O₅/G heterostructures and rechargeable battery chemistry of A-V₂O₅/G-ZIBs. (a) The synthetic scheme of 2D A-V₂O₅/G heterostructures. (b,c) Schematic diagram of the (b) discharging and (c) charging states of A-V₂O₅/G-ZIBs with Zn anode and A-V₂O₅/G cathode.

heterostructures assembled with 2D ultrathin, high-capacity, amorphous cathode (e.g., V₂O₅) in a controllable layer-by-layer stacked order, which may efficiently enhance electron transfer, alleviate volume expansion and achieve the performance improvement due to the strong synergy, stable disordered structure, rich defects and 2D laminar confinement [29]. Notably, such 2D layer-by-layer heterostructures promise high accessible surface area, nearly 100% utilization of active materials, rapid electron transport in conducting nanosheets, and fast ion diffusion in the lamellar permeable spaces, which are desirable for achieving high capacity and long-term cyclability of ZIBs. But the creation of such well-defined layer-stacked 2D heterostructures from ultrathin high-capacity V₂O₅ and conducting graphene with strong coupling for aqueous ZIBs has not yet been achieved.

Herein, we report a novel 2D template ion adsorption strategy for the controlled assembly of layer-by-layer stacked amorphous V₂O₅/graphene (A-V₂O₅/G) 2D heterostructures with strong-coupling effect for high-performance aqueous ZIBs (denoted as A-V₂O₅/G-ZIBs). Owing to the advantageous nature of amorphous, ultrathin V₂O₅ layer with numerous active sites and minimized volume change confined by 2D flexible graphene in the heterostructures, the as-assembled A-V₂O₅/G-ZIBs possess abundant electron transport pathways in conducting graphene, and short ion diffusion distances in 2D lamellar nanochannels. Remarkably, the resulting A-V₂O₅/G-ZIBs deliver high capacity of 447 mAh/g at 0.3 A/g, extraordinary rate capability of 202 mAh/g at 30 A/g, and unprecedented ultra-long life with capacity retention of 83% after 20,000 cycles at 30 A/g. Such high capacity and ultra-long cyclability have never been obtained at the same time in the reported ZIBs. Additionally, the planar

zinc ion micro-batteries (referred as A-V₂O₅/G-ZIMBs) with interdigital asymmetric microelectrodes of Zn anode and A-V₂O₅/G cathode are successfully assembled in a single substrate through mask-assisted filtration. The as-assembled A-V₂O₅/G-ZIMBs display impressive volumetric capacity of 57 mAh/cm³ at 0.2 mA/cm², splendid energy density of 45 mWh/cm³, long lifespan up to 1500 cycles and satisfactory serial/parallel self-integration. Moreover, the planar A-V₂O₅/G-ZIMBs exhibit eminent flexibility and capacity retention under different bending states.

2. Experimental

2.1. Preparation of 2D A-V₂O₅/G heterostructures

Firstly, a dark blue solution of VOC₂O₄ was made by dissolving 2 mM V₂O₅ (Sigma-Aldrich) and 6 mM H₂C₂O₄ (Sigma-Aldrich) into distilled water at 75 °C for 2 h. Then, the single-layer GO (1 mg/mL, 80 mL) nanosheets were used as 2D templates to adsorb the VOC₂O₄ monomers (9.6 mL). After that, the resultant solution was dried at 60 °C for 24 h. Finally, the dried sample was annealed at 300 °C for 2 h to obtain 2D A-V₂O₅/G heterostructures. For comparison, 2D crystal V₂O₅/graphene (C-V₂O₅/G) was prepared by annealing at 450 °C, and crystal V₂O₅ (C-V₂O₅) was synthesized without GO, while other steps were kept the same as 2D A-V₂O₅/G.

2.2. Fabrication of A-V₂O₅/G-ZIBs and A-V₂O₅/G-ZIMBs

The stacked A-V₂O₅/G ZIBs were constructed in 2016 coin cells based

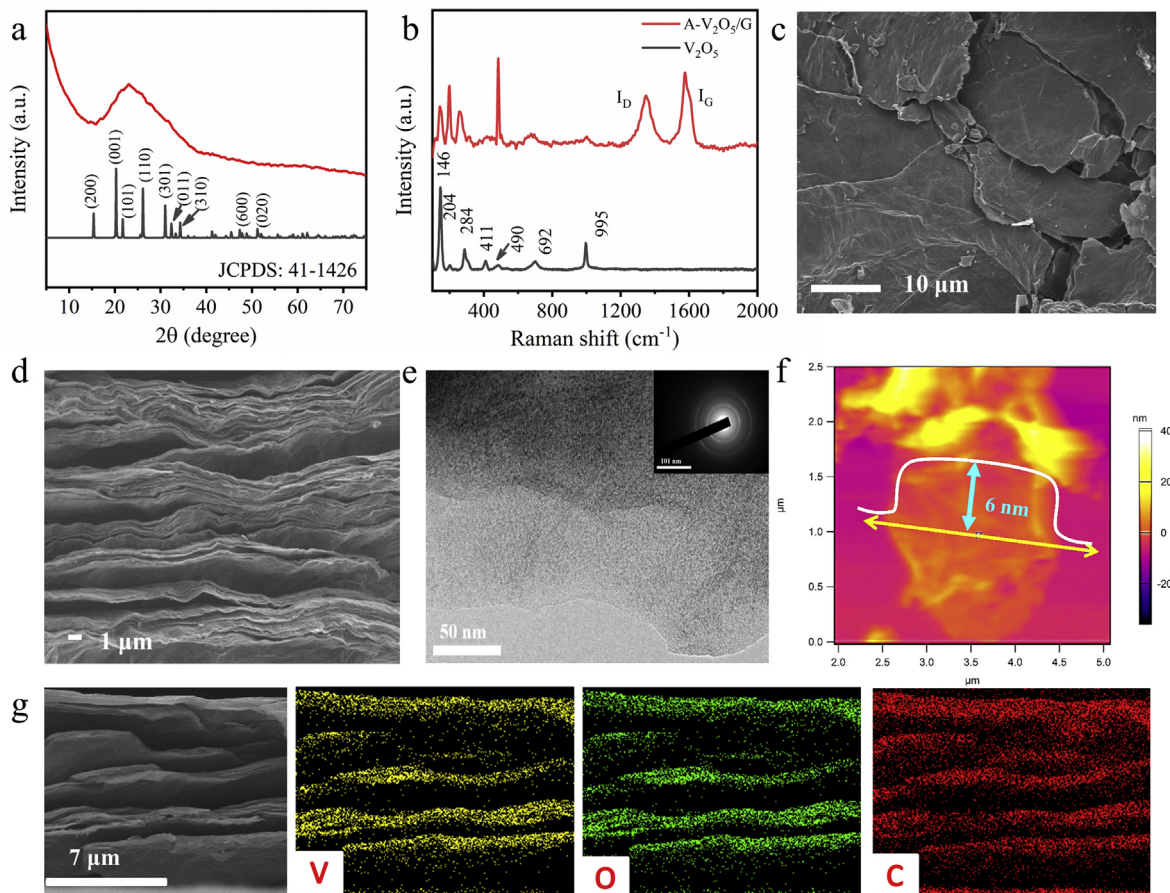


Fig. 2. Morphological and structural characterizations of 2D A-V₂O₅/G heterostructure. (a) XRD patterns and (b) Raman spectra of A-V₂O₅/G and V₂O₅. (c) Top-view and (d) cross-section SEM images of A-V₂O₅/G heterostructures. (e) HRTEM image and SAED pattern (inset) of A-V₂O₅/G. f) AFM image and height profile (inset) of A-V₂O₅/G heterostructure on a silicon wafer. (g) Cross-section EDX mapping of V, O and C elements on 2D A-V₂O₅/G heterostructures.

on 2D A-V₂O₅/G as cathode, zinc foil as anode, 3 M ZnSO₄ (V₂O₅ sol) as electrolyte, and glass fiber membrane as separator. The cathode was composed of 80 wt% A-V₂O₅/G, 10 wt% polyvinylidene difluoride binder, and 10 wt% acetylene black, and loaded on a stainless steel foil (0.01 mm thick) and dried at 80 °C for 12 h.

The planar A-V₂O₅/G-ZIMBs were fabricated by mask-assisted vacuum filtration [30–32]. Firstly, high quality electrochemically exfoliated graphene (EG, Fig. S1) ethanol dispersion (0.1 mg/mL, 1 mL) was filtrated through the interdigital home-made mask with eight fingers (length of 14 mm, width of 1 mm, interspace of 0.5 mm). Then, A-V₂O₅/G (0.5 mg/mL, 10 wt% EG) and zinc powder (0.5 mg/mL, 10 wt% EG) ethanol dispersions were filtrated in sequence onto the each side of the fingers (four fingers) with assistance of the customized interdigital mask. Afterwards, 3 M ZnSO₄ (V₂O₅ sol) electrolyte was carefully dropped onto the projected area of interdigital microelectrodes. Finally, the planar A-V₂O₅/G-ZIMBs were achieved after package.

2.3. Materials characterization

The morphology, structure and composition of the active materials, graphene, and microelectrodes were characterized using field-emission SEM (JSM-7800F), HRTEM (JEM-2100), XRD (X'pert Pro)(5° - 90°), XPS (Omicron Multiprobe equipped with the monochromatic Al $K\alpha$ source, electron analyzer resolution of 0.9 eV), AFM (MultiMode 3D microscopy), Raman spectrometer (LabRAM HR800), and thermogravimetric analysis (TGA, STA 449 F3, measured at air atmosphere, 10°/min from 25 to 650 °C).

2.4. Electrochemical measurement

The CV curves obtained at varying scan rates of 1–9 mV/s and EIS tested from 100 kHz to 0.01 Hz with an AC amplitude of 5 mV were conducted by an electrochemical workstation (CHI 760E), and the GCD profiles were measured by LAND CT2001A battery tester at the voltage of between 0.2 and 1.8 V at different current densities from 0.3 to 30 A/g.

3. Results and discussion

The layer-by-layer A-V₂O₅/G heterostructures were assembled by 2D graphene oxide (GO) template-based ion adsorption approach, as schematically illustrated in Fig. 1a (See details in Experimental Section). Briefly, hydrothermal reaction of V₂O₅ with H₂C₂O₄ was applied to form the VO₂C₂O₄, adsorbing onto both sides of GO. After annealing, the A-V₂O₅/G heterostructures were obtained. It is noted that such 2D compact heterostructures with layer-by-layer stacked skeleton and lamellar amorphous V₂O₅ nanosheets are favorable for the fast and reversible storage of zinc ions (Fig. 1b–c). X-ray diffraction (XRD) pattern of A-V₂O₅/G heterostructures (Fig. 2a) showed a broad peak at 23° derived from layer-by-layer stacking of graphene, and the absence of other peaks, demonstrative of the amorphous framework of V₂O₅. Raman spectrum evidenced the characteristic peaks of the vibration of V–O bonds at 115, 141, 198, 272, 484, 688, and 997 cm⁻¹ [18,33] and D peak at 1348 cm⁻¹ and G peak at 1577 cm⁻¹ for graphene (Fig. 2b), suggestive of the co-existence of V₂O₅ and graphene in 2D heterostructures. Importantly, scanning electron microscopy (SEM) images (Fig. 2c–d), represented a layer-by-layer stacking yet compact feature of the alternative graphene

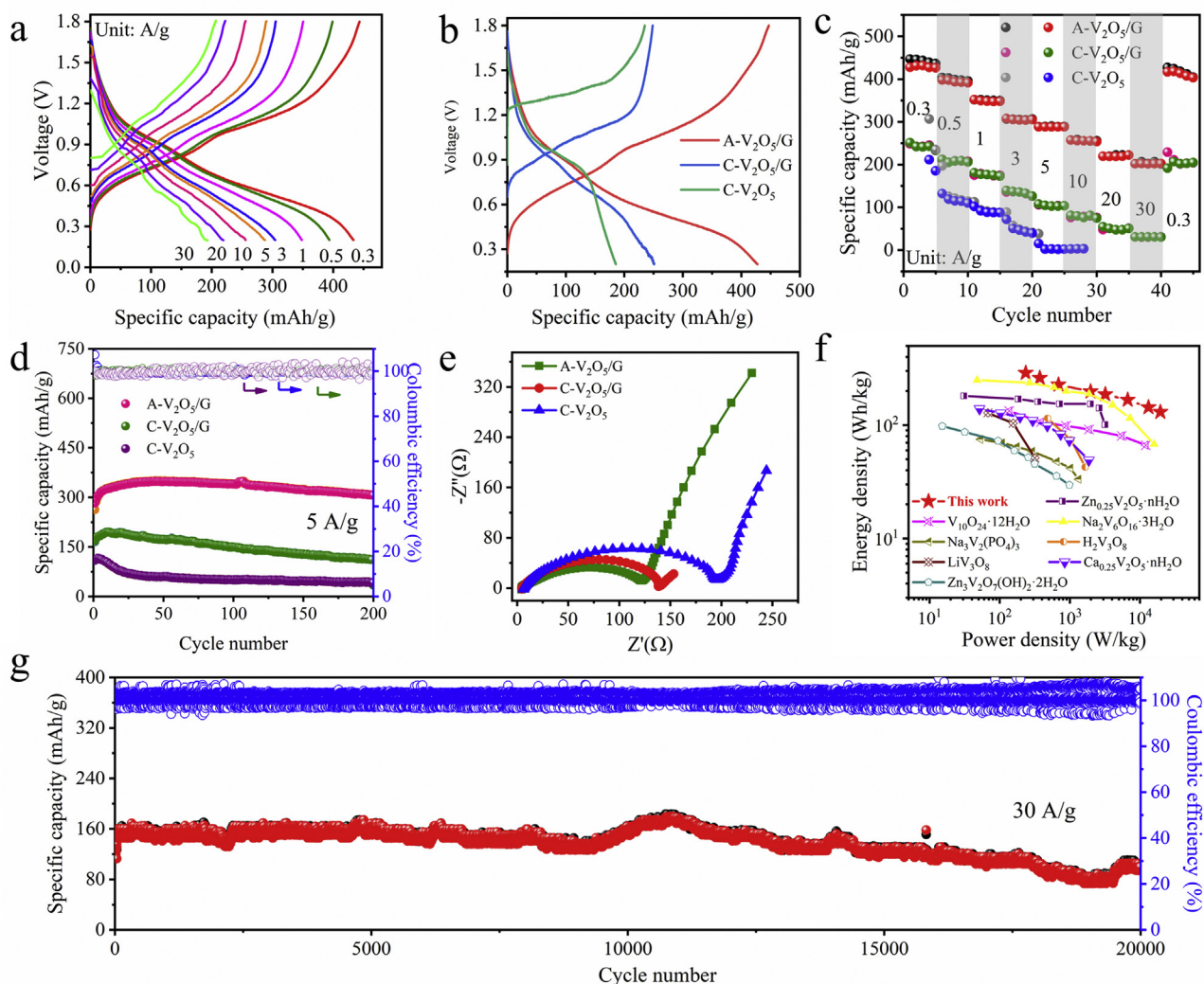


Fig. 3. Electrochemical performance of A-V₂O₅/G-ZIBs. (a) The GCD profiles measured at different current densities ranging from 0.3 to 30 A/g of A-V₂O₅/G-ZIBs. (b) GCD profiles tested at 0.3 A/g of A-V₂O₅/G-ZIBs, C-V₂O₅/G-ZIBs, and C-V₂O₅-ZIBs. (c) Rate capability of A-V₂O₅/G-ZIBs, obtained from 0.3 to 30 A/g. (d) The cyclability tested at 5 A/g and (e) EIS curves of A-V₂O₅/G-ZIBs, C-V₂O₅/G-ZIBs, and C-V₂O₅-ZIBs. (f) Ragone plot of A-V₂O₅/G-ZIBs and some reported aqueous ZIBs based on different cathode materials. (g) Long-term cyclability of A-V₂O₅/G-ZIBs tested at high current density of 30 A/g for 20,000 cycles.

and amorphous V₂O₅ in 2D heterostructures. Besides, high-resolution transmission electron microscopy (HRTEM) image and selected area electron diffraction (SAED) image displayed the uniform amorphous V₂O₅ closely anchored onto graphene (Fig. 2e, Fig. S2), and atomic force microscope (AFM) image confirmed the uniform thickness of 6 nm (Fig. 2f). Elemental mapping analysis revealed the homogeneous distribution of V, O, and C elements in A-V₂O₅/G heterostructure (Fig. 2g). The content of graphene in this heterostructure was evaluated to be ~38% (Fig. S3) [10]. It is worth noting that graphene in the 2D heterostructure plays important roles in dramatically enhancing the electrical conductivity and alleviating the volume change of ultrathin amorphous V₂O₅ layer, contributing to fast kinetics and stable structure during Zn²⁺ ions storage.

To examine the electrochemical performance of 2D A-V₂O₅/G heterostructures as cathode, the A-V₂O₅/G-ZIBs were assembled, using Zn foil as anode and 3 M ZnSO₄ (V₂O₅ sol) as aqueous electrolyte. To emphasize the superiority of amorphous structure over crystalline V₂O₅ and validate the importance of graphene, the counterparts of ZIBs based on 2D heterostructure cathodes of crystalline V₂O₅ anchored on graphene (C-V₂O₅/G-ZIBs, Figs. S4a–c) and crystalline V₂O₅ nanosheets without graphene (C-V₂O₅-ZIBs, Figs. S4d–f) were also fabricated for comparison. The galvanostatic charge-discharge (GCD, Fig. 3a) profiles

showed two couple of reversible voltage plateaus located at 0.55/0.88 V and 0.83/1.1 V, which could be ascribed to the proportionally multiple Zn²⁺ ion insertion/extraction process [34,35]. Impressively, at low current density of 0.3 A/g, A-V₂O₅/G-ZIBs delivered a record capacity of 447 mAh/g (Fig. 3b), which was much higher than those of C-V₂O₅/G-ZIBs (202 mAh/g) and V₂O₅-ZIBs (185 mAh/g), and the reported ZIBs, such as $Zn_{0.25}V_2O_5 \cdot nH_2O$ (282 mAh/g at 1C) [9], $Ca_{0.25}V_2O_5 \cdot nH_2O$ (340 mAh/g at 0.2C) [36], $H_2V_3O_8$ (423.8 mAh/g at 0.1 A/g) [37]. With increased current densities, A-V₂O₅/G-ZIBs disclosed average discharge capacities of 404, 352, 306, 289, 259, 222, and 202 mAh/g at the current densities of 0.5, 1, 3, 5, 10, 20, and 30 A/g, respectively (Fig. 3c). On a sharp contrast, C-V₂O₅/G-ZIBs showed lower capacities of 81 mAh/g at 10 A/g and 31 mAh/g at 30 A/g, and C-V₂O₅-ZIBs only operated at a maximum current density of 10 A/g, displaying a much lower capacity of 3 mAh/g. The enhanced rate capability of A-V₂O₅/G-ZIBs and C-V₂O₅/G-ZIBs compared with C-V₂O₅-ZIBs was a result from the high electrical conductivity of graphene. Remarkably, after the current density suddenly returned to 0.3 A/g, A-V₂O₅/G-ZIBs readily recovered to a higher capacity of 418 mAh/g than that (207 mAh/g) of C-V₂O₅/G-ZIBs, implying the superiority of amorphous over crystalline phase of V₂O₅ in 2D heterostructures. Moreover, A-V₂O₅/G-ZIBs presented highly stable cycling performance with an

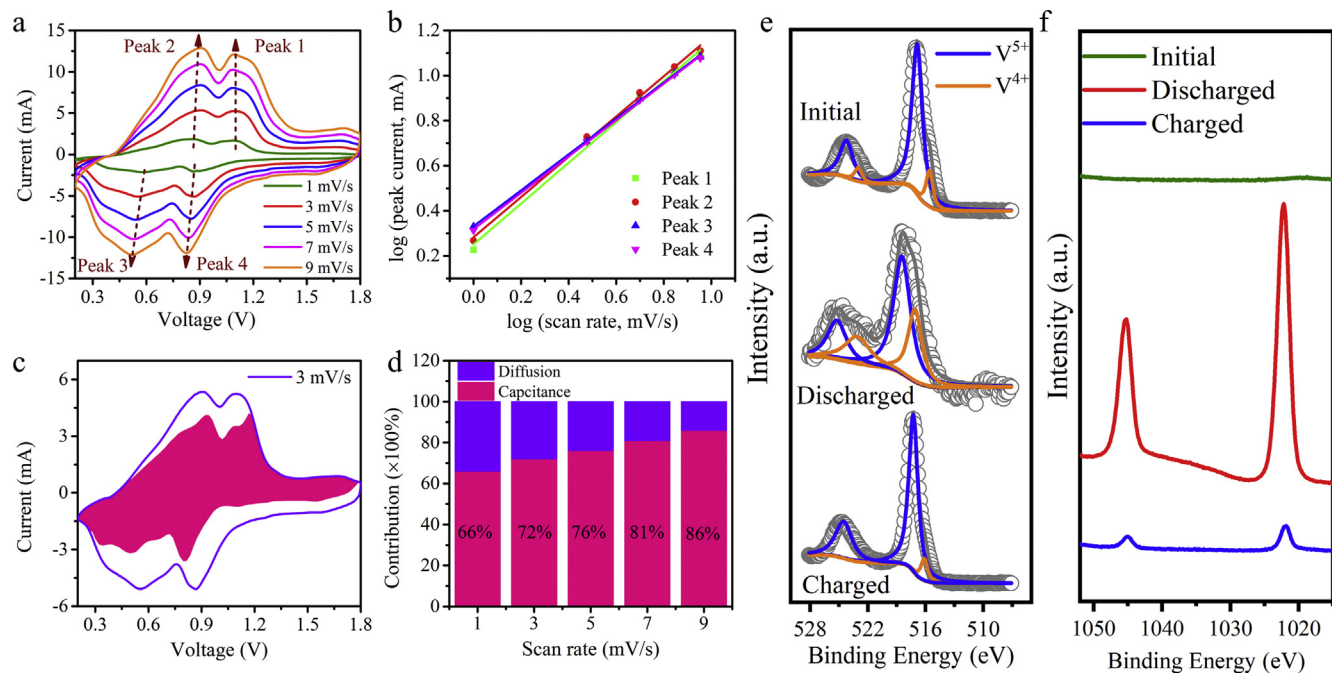


Fig. 4. Kinetics analysis and reaction mechanism of A-V₂O₅/G-ZIBs. (a) CV curves tested at different scan rates from 1 to 9 mV/s. (b) The plots of log (*i*) versus log (*v*) of cathodic and anodic peaks. (c) Capacitive contribution (pink part) and diffusion-controlled contribution (void part) at 3.0 mV/s. (d) Normalized capacity contribution ratios from capacitive (pink part) and diffusion-controlled (purple part) process from 1 to 9 mV/s. (e) V 2p_{3/2} and (f) Zn 2p_{3/2} XPS spectra of 2D A-V₂O₅/G cathode at pristine, fully discharged (0.2 V) and charged states (1.8 V). (For interpretation of the references to colour in this figure legend, the reader is referred to the Web version of this article.)

extraordinary retention of 100% after 200 cycles at 5 A/g (Fig. 3d, Fig. S5a), compared to C-V₂O₅/G-ZIBs (31%) and C-V₂O₅-ZIBs (67%) as well as graphene for ZIBs (Figs. S5b–c). This result was further explained by electrochemical impedance spectroscopy (EIS, Fig. 3e, Figs. S6a–b), in which A-V₂O₅/G-ZIBs revealed the lower charge transfer resistance (R_{ct}) of 130 Ω, much lower than those of C-V₂O₅/G-ZIBs (174 Ω) and C-V₂O₅-ZIBs (185 Ω). Further, the energy density of A-V₂O₅/G-ZIBs based on the mass of A-V₂O₅/G cathode was calculated to be as high as 288 Wh/kg at a power density of 234 W/kg (Fig. 3f). This value is superior to the-state-of-art ZIBs reported, for example, based on the cathodes of V₁₀O₂₄·12H₂O (133 Wh/kg) [38], Zn_{0.25}V₂O₅·nH₂O (181 Wh/kg) [9], Na₂V₆O₁₆·3H₂O (249 Wh/kg) [39], Na₃V₂(PO₄)₃ (75 Wh/kg) [40], H₂V₃O₈ (115 Wh/kg) [37], LiV₃O₈ (128 Wh/kg) [41], Ca_{0.25}V₂O₅·nH₂O (139 Wh/kg) [36] and Zn₃V₂O₇(OH)₂·2H₂O (98 Wh/kg) [26]. Even at high current density of 30 A/g, corresponding to an extremely short discharge time of 24 s, A-V₂O₅/G-ZIBs delivered an impressive power density of 19.5 kW/kg and simultaneously energy density of 130 Wh/kg.

Furthermore, A-V₂O₅/G-ZIBs exhibited unprecedented ultra-long cycling stability with capacity retention of ~83% after 20,000 cycles (Fig. 3g, Fig. S7), suppressing C-V₂O₅/G-ZIBs (56%) and C-V₂O₅-ZIBs (46%) after 4000 cycles (Fig. S8), and most of the reported ZIBs, such as Zn₃V₂O₇(OH)₂·2H₂O ZIBs (68% retention after 300 cycles) [26], V₂O₅·nH₂O ZIBs (71% after 900 cycles) [10], Li_xV₂O₅·nH₂O ZIBs (64% after 1000 cycles) [19] (Table S1). Such long cycle life was mainly attributed to the unique 2D heterostructure of layer-by-layer stacked amorphous V₂O₅ and conducting graphene, where amorphous V₂O₅ offered tremendous available active sites, and graphene greatly enhanced the electrical conductivity and alleviated the volume change of ultrathin amorphous V₂O₅, guaranteeing the extraordinarily stable skeleton structure for rapid electron transport and ion diffusion during the repeated (de)intercalation of Zn²⁺ ions. In addition, the concentration of electrolyte also had a great impact on the performance of A-V₂O₅/G-ZIBs (Fig. S9).

To gain further insight into the kinetics in A-V₂O₅/G-ZIBs, cyclic voltammetry (CV) test with increasing scan rates from 1 to 9 mV/s

(Fig. 4a) was carried out. The total storage charge could be divided into three components [42,43], including the faradaic contribution from Zn²⁺ insertion process, the faradaic contribution from the surface redox process (referred to pseudocapacitance), and the nonfaradaic contribution. The latter two components cannot be distinguished efficiently and can be described together by the equation $i = a v^b$, where a and b are adjustable parameters and the value of b reflects the dominated process modes. In principle, $b = 0.5$ represents the diffusion-controlled insertion process while $b = 1$ indicates the surface process [11,12]. For A-V₂O₅/G-ZIBs, the b values were calculated to be 0.9 (peak 1), 0.89 (peak 2), 0.8 (peak 3), and 0.81 (peak 4), respectively (Fig. 4b), implying the co-existence of both diffusion-controlled and capacitive process. Furthermore, the contributions to the total capacity of A-V₂O₅/G-ZIBs was evaluated by the formula $i(V) = k_1 v + k_2 v^{1/2}$, where the $k_1 v$ and $k_2 v^{1/2}$ correspond to the current contributions arising from the surface capacitive effects and the diffusion-controlled processes, respectively [44]. Remarkably, 72% of the capacity was attributed to the capacitive response at 3 mV/s. Moreover, it can be seen that the capacitive contribution increased steadily with the increase of scan rates (Fig. 4d), which played a dominating role in the total capacity devoted to the enlarged rate performance.

To probe the reaction mechanism of A-V₂O₅/G-ZIBs, the *ex-situ* X-ray photoelectron spectroscopy (XPS) was carried out. Apparently, the pristine A-V₂O₅/G cathode was fitted into two peaks, one big V 2p_{3/2} peak at 517 eV (Fig. 4e) corresponding to V⁵⁺ species, and a weak V 2p_{1/2} peak at 514 eV resulting from slight reduction by oxygenated graphene during synthesis [26]. After being discharged to 0.2 V, it is observed that the peak intensity of V⁵⁺ signal decreased while the V⁴⁺ increased (Fig. 4e), indicative of partial reduction from V⁵⁺ to V⁴⁺. Importantly, the pristine V 2p XPS was recovered upon charging, manifesting high reversibility. Accordingly, the appearance of both Zn 2p_{3/2} (1022.04 eV) and Zn 2p_{1/2} (1045.19 eV) [45] strong peaks was demonstrative of Zn²⁺ insertion and outstanding reversibility (Fig. 4f) [46]. In addition, it is revealed that from the *ex-situ* XRD patterns and HRTEM images (Fig. S10) there was no insertion of H⁺ ions into the A-V₂O₅/G cathode for ZIBs during discharge process [47–49].

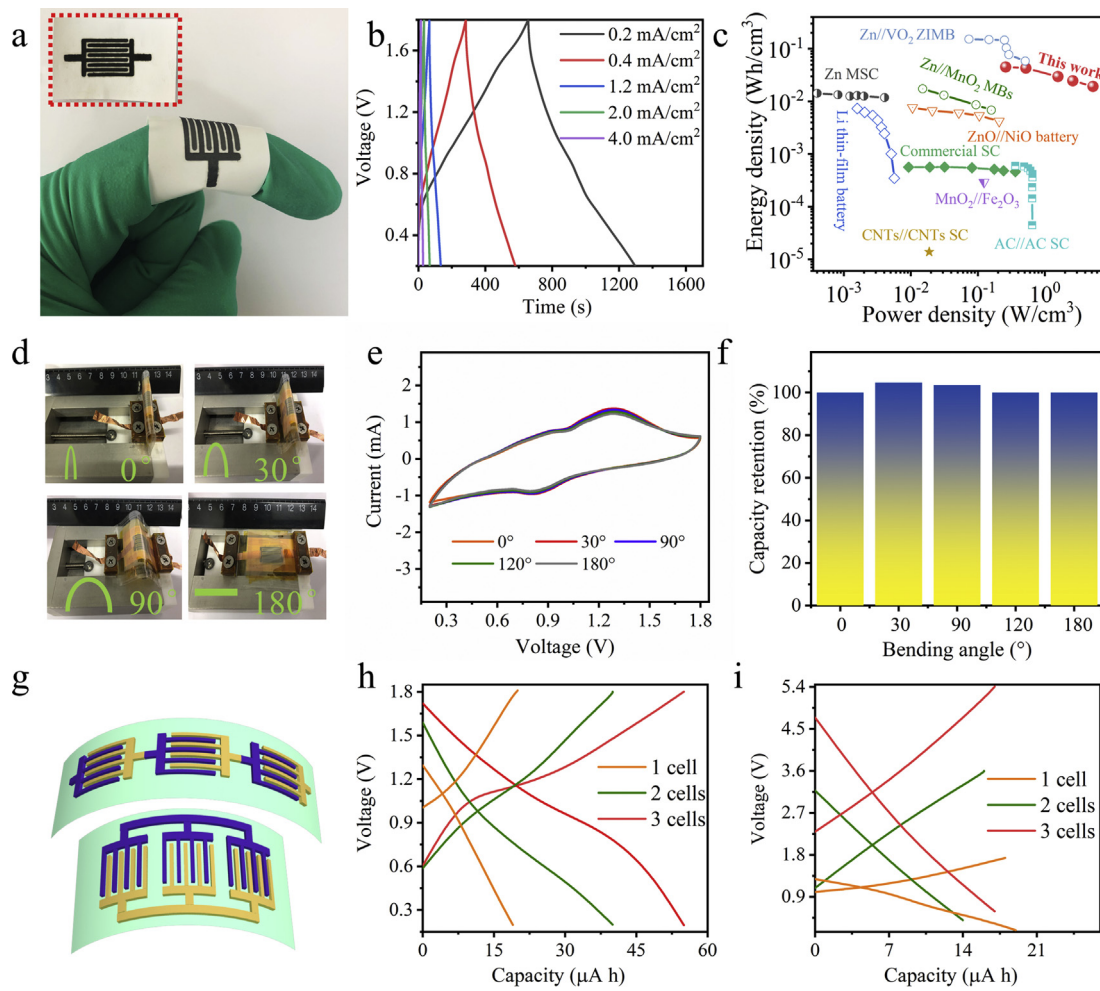


Fig. 5. Electrochemical performance of planar A-V₂O₅/G-ZIMBs. (a) Photographs of as-assembled planar A-V₂O₅/G-ZIMBs on the PTFE membrane (inset: a flat state) attached on the bending finger. (b) GCD profiles of A-V₂O₅/G-ZIMBs obtained at different current densities of 0.4, 1.2, 2 and 4 mA/cm². (c) Ragone plot of A-V₂O₅/G-ZIMBs compared with other microscale energy-storage devices (AC: active carbon, CNTs: carbon nanotubes). (d) Photographs of A-V₂O₅/G-ZIMBs taken at different bending states. (e) The corresponding CV curves measured at 30 mV/s and (f) capacity retention of A-V₂O₅/G-ZIMBs at different bending angles. (g) Schematic illustration of the integrated planar A-V₂O₅/G-ZIMBs connected three cells in series (up) and in parallel (bottom). (h,i) GCD profiles of the integrated planar A-V₂O₅/G-ZIMBs connected (h) in parallel and (i) in series from 1 to 3 cells.

To satisfy the urgent demand of the wearable and miniaturized electronics, the new-concept, high-safety, planar A-V₂O₅/G-ZIMBs were further constructed based on interdigital asymmetric microelectrodes of 2D A-V₂O₅/G heterostructures as cathode and Zn nanopowder as anode on one single substrate by mask-assisted vacuum filtration strategy (See details in Experimental Section) [30]. It can be observed that the interdigital microelectrodes of A-V₂O₅/G-ZIMBs (Fig. 5a) showed impressively mechanical flexibility attached to flexible human fingers. SEM images exhibited the uniform thickness of ~6 μm for A-V₂O₅/G cathode and ~5 μm for Zn anode (Fig. S11). Moreover, A-V₂O₅/G-ZIMBs displayed a remarkable capacity of 63 mAh/cm³ at 0.2 mA/cm², and excellent rate capability of 60, 41, 35, and 27 mAh/cm³ at 0.4, 1.2, 2, and 4 mA/cm², respectively, together with good cyclability with capacity retention of 85% after 1500 cycles (Fig. S12). Remarkably, A-V₂O₅/G-ZIMBs presented high volumetric power density of 5.7 W/cm³ and volumetric energy density of 49 mWh/cm³ (Fig. 5c), outperforming most of the reported micro-electrochemical energy storage devices, such as commercially available micro-supercapacitors (MSCs, 1 mWh/cm³) [50], Zn-ion MSCs (ZIMSCs, 11.81 mWh/cm³) [50], lithium thin-film micro-batteries (MBs, 10 mWh/cm³) [51], ZnO//NiO MBs (11 mWh/cm³) [52], and Zn//MnO₂ MBs (17 mWh/cm³) [53]. Further, the shapes of CV curves of A-V₂O₅/G-ZIMBs well overlapped at different bending angles (Fig. 5d–e), verifying outstanding flexibility and electrochemical stability

(Fig. 5f). It's noteworthy that the A-V₂O₅/G-ZIMBs featured excellent serial and parallel integration (Fig. 5g). For instance, the integrated A-V₂O₅/G-ZIMBs displayed a stepwise increase in output capacity from ~18 μAh for single cell to ~36 μAh for two cells, and ~54 μAh for three cells in parallel (Fig. 5h). Meanwhile, the voltage in series fashion exhibited a linear increase from ~0.9 V for single cell to ~1.8 V for two cells and ~2.7 V for three cells (Fig. 5i, S13a-b), demonstrative of exceptional performance uniformity. Two serially connected A-V₂O₅/G-ZIMBs could easily light up a light-emitting diode (LED) for a significantly long time under the bending state, and power a display screen of our institute “DICP” logo (Fig. S14). These results validated the great potential of ZIMBs and their integrated micro-power sources for high-energy and high-voltage wide applicability in the microelectronics and other microsystems.

The extraordinary performance of A-V₂O₅/G-ZIMBs was mainly attributed to the synergistic effect of 2D A-V₂O₅/G heterostructures with unique layer-by-layer stacking structures of uniform amorphous V₂O₅ framework and conducting graphene. Firstly, the ultrathin amorphous V₂O₅ structure with inherent disorderliness in the structural arrangement and rich defects, has enriched active sites, reduces the ion diffusion length and high chemical stability, resulting in the satisfactory performance [54]. Secondly, 2D electrically conducting graphene could not only serve as a 2D flexible substrate for the uniform growth of amorphous

V_2O_5 framework, but also significantly promote the fast electron transport of the V_2O_5 layers at nanoscale. Thirdly, 2D heterostructures combine the intriguing merits of highly accessible surface area, superior electrical conductivity, rapid electron transport in conducting nanosheets, and fast ion diffusion in the lamellar permeable spaces, leading to high capacity and rate capability [29]. Fourth, the layer-by-layer stacked heterostructures render facile alleviation of the strains caused by ion insertion and extraction and effectively relieve the dissolution of the V_2O_5 due to the compact layer-by-layer structure, which effectively maximizes the capacity and cyclability of amorphous V_2O_5 [55]. Last but not least, the new-concept planar ZIMBs are free of separator, metal current collectors and conventional polymer binders, and also possess extremely short ion diffusion pathways and developed electron transport distances, contributing to the impressive performance, flexibility and cell modular integration [56].

4. Conclusions

In summary, we demonstrated the successful construction of high-safety, aqueous A- V_2O_5 /G-ZIBs with remarkable capacity of 447 mAh/g at 0.3 A/g, and ultra-long cycle life up to 20,000 cycles, based on 2D layer-by-layer stacked amorphous A- V_2O_5 /G heterostructures with vast active sites, high electrical conductivity, and short ion diffusion. The resultant aqueous A- V_2O_5 /G-ZIBs overcome the traditional challenging issues of lithium ion batteries with flammable toxic electrolyte and the reported ZIBs with limited capacity and poor cyclability. Moreover, the as-fabricated planar A- V_2O_5 /G-ZIMBs displayed high energy density of 49 mWh/cm³, exceptional flexibility, and satisfactory integration. The layer-by-layer 2D heterostructures can allow for the fast ion diffusion for amorphous ultrathin V_2O_5 structure and speeded electron transport from highly conductive graphene for high-performance A- V_2O_5 /G-ZIBs. Therefore, this work not only provides a new strategy for protecting the active material from dissolution in the layer-by-layer structure, but also will open up many novel opportunities for developing high-safe aqueous ZIBs with high performance, miniaturization, and other form factors, holding great promise in the low-cost applications of large-scale energy storage and microelectronics.

Declaration of competing interest

There are no conflicts to declare.

CRediT authorship contribution statement

Xiao Wang: Conceptualization, Methodology, Data curation, Writing - original draft. **Yuguang Li:** Conceptualization, Methodology, Data curation, Writing - original draft. **Pratteek Das:** Writing - review & editing. **Shuanghao Zheng:** Writing - review & editing. **Feng Zhou:** Conceptualization, Resources. **Zhong-Shuai Wu:** Writing - review & editing.

Acknowledgments

This work was financially supported by the National Natural Science Foundation of China (Grants 51572259, 51872283, 21805273), National Key R&D Program of China (Grants 2016YFB0100100, 2016YFA0200200), Liaoning BaiQianWan Talents Program, LiaoNing Revitalization Talents Program (Grant XLYC1807153), Natural Science Foundation of Liaoning Province, Joint Research Fund Liaoning-Shenyang National Laboratory for Materials Science (Grant 20180510038), DICP (DICP ZZBS201708, DICP ZZBS201802), DICP&QIBET (Grant DICP&QIBET UN201702), Dalian National Laboratory For Clean Energy (DNL), CAS, DNL Cooperation Fund, CAS (DNL180310, DNL180308, DNL201912, DNL201915).

Appendix A. Supplementary data

Supplementary data to this article can be found online at <https://doi.org/10.1016/j.ensm.2020.06.010>.

References

- [1] M. Armand, J.M. Tarascon, Building better batteries, *Nature* 451 (2008) 652–657.
- [2] M. Song, H. Tan, D. Chao, H.J. Fan, Recent advances in Zn-ion batteries, *Adv. Funct. Mater.* 28 (2018) 1802564.
- [3] A. Konarov, N. Voronina, J.H. Jo, Z. Bakenov, Y.K. Sun, S.T. Myung, Present and future perspective on electrode materials for rechargeable zinc-ion batteries, *ACS Energy Lett.* 3 (2018) 2620–2640.
- [4] G.Z. Fang, J. Zhou, A.Q. Pan, S.Q. Liang, Recent advances in aqueous zinc-ion batteries, *ACS Energy Lett.* 3 (2018) 2480–2501.
- [5] Y. Li, J. Fu, C. Zhong, T. Wu, Z. Chen, W. Hu, K. Amine, J. Lu, Recent advances in flexible zinc-based rechargeable batteries, *Adv. Energy Mater.* 9 (2019) 1802605.
- [6] L. Suo, O. Borodin, Y. Wang, X. Rong, W. Sun, X. Fan, S. Xu, M.A. Schroeder, A.V. Cresce, F. Wang, C. Yang, Y.-S. Hu, K. Xu, C. Wang, “Water-in-Salt” electrolyte makes aqueous sodium-ion battery safe, green, and long-lasting, *Adv. Energy Mater.* 7 (2017) 1701189.
- [7] L.W. Jiang, Y.X. Lu, C.L. Zhao, L.L. Liu, J.N. Zhang, Q.Q. Zhang, X. Shen, J.M. Zhao, X.Q. Yu, H. Li, X.J. Huang, L.Q. Chen, Y.S. Hu, Building aqueous K-ion batteries for energy storage, *Nat. Energy* 4 (2019) 495–503.
- [8] J. Huang, Z. Guo, Y. Ma, D. Bin, Y. Wang, Y. Xia, Recent progress of rechargeable batteries using mild aqueous electrolytes, *Small Methods* 3 (2018) 1800272.
- [9] D. Kundu, B.D. Adams, V. Duffort, S.H. Vajargah, L.F. Nazar, A high-capacity and long-life aqueous rechargeable zinc battery using a metal oxide intercalation cathode, *Nat. Energy* 1 (2016) 16119.
- [10] M. Yan, P. He, Y. Chen, S. Wang, Q. Wei, K. Zhao, X. Xu, Q. An, Y. Shuang, Y. Shao, K.T. Mueller, L. Mai, J. Liu, J. Yang, Water-lubricated intercalation in $V_2O_5\cdot nH_2O$ for high-capacity and high-rate aqueous rechargeable zinc batteries, *Adv. Mater.* 30 (2018) 1703725.
- [11] D. Chao, C.R. Zhu, M. Song, P. Liang, X. Zhang, N.H. Tiep, H. Zhao, J. Wang, R. Wang, H. Zhang, H.J. Fan, A high-rate and stable quasi-solid-state zinc-ion battery with novel 2D layered zinc orthovanadate array, *Adv. Mater.* 30 (2018) 1803181.
- [12] Y. Jin, L. Zou, L. Liu, M.H. Engelhard, R.L. Patel, Z. Nie, K.S. Han, Y. Shao, C. Wang, J. Zhu, H. Pan, J. Liu, Joint charge storage for high-rate aqueous zinc-manganese dioxide batteries, *Adv. Mater.* 31 (2019) 1900567.
- [13] J. Huang, Z. Wang, M. Hou, X. Dong, Y. Liu, Y. Wang, Y. Xia, Polyaniiline-intercalated manganese dioxide nanolayers as a high-performance cathode material for an aqueous zinc-ion battery, *Nat. Commun.* 9 (2018) 2906.
- [14] W. Sun, F. Wang, S. Hou, C. Yang, X. Fan, Z. Ma, T. Gao, F. Han, R. Hu, M. Zhu, C. Wang, Zn/MnO₂ battery chemistry with H⁺ and Zn²⁺ coininsertion, *J. Am. Chem. Soc.* 139 (2017) 9775–9778.
- [15] Q. Yang, F. Mo, Z. Liu, L. Ma, X. Li, D. Fang, S. Chen, S. Zhang, C. Zhi, Activating C-coordinated iron of iron hexacyanoferrate for Zn hybrid-ion batteries with 10 000-cycle lifespan and superior rate capability, *Adv. Mater.* 31 (2019) 1901521.
- [16] P. Hu, T. Zhu, X. Wang, X. Zhou, X. Wei, X. Yao, W. Luo, C. Shi, K.A. Owusu, L. Zhou, L. Mai, Aqueous Zn//Zn(CF₃SO₃)₂//Na₃V₂(PO₄)₃ batteries with simultaneous Zn²⁺/Na⁺ intercalation/de-intercalation, *Nano Energy* 58 (2019) 492–498.
- [17] F. Wan, Y. Zhang, L. Zhang, D. Liu, C. Wang, L. Song, Z. Niu, J. Chen, Reversible oxygen redox chemistry in aqueous zinc-ion batteries, *Angew. Chem. Int. Ed.* 58 (2019) 7062–7067.
- [18] P. He, G. Zhang, X. Liao, M. Yan, X. Xu, Q. An, J. Liu, L. Mai, Sodium ion stabilized vanadium oxide nanowire cathode for high-performance zinc-ion batteries, *Adv. Energy Mater.* 8 (2018) 1702463.
- [19] Y. Yang, Y. Tang, G. Fang, L. Shan, J. Guo, W. Zhang, C. Wang, L. Wang, J. Zhou, S. Liang, Li⁺ intercalated $V_2O_5\cdot nH_2O$ with enlarged layer spacing and fast ion diffusion as an aqueous zinc-ion battery cathode, *Energy Environ. Sci.* 11 (2018) 3157–3162.
- [20] K. Zhu, T. Wu, K. Huang, NaCa_{0.6} $V_6O_{16}\cdot 3H_2O$ as an ultra-stable cathode for Zn-ion batteries: the roles of pre-inserted dual-cations and structural water in V_3O_8 layer, *Adv. Energy Mater.* 9 (2019) 1901968.
- [21] K.-W.H. Lulu Wang, Jitao Chen, Junrong Zheng, Ultralong cycle stability of aqueous zinc-ion batteries with zinc vanadium oxide cathodes, *Sci. Adv.* 5 (2019), eaax4279.
- [22] Y. Cai, F. Liu, Z. Luo, G. Fang, J. Zhou, A. Pan, S. Liang, Pilotaxitic Na_{1.1}V₃O_{7.9} nanoribbons/graphene as high-performance sodium ion battery and aqueous zinc ion battery cathode, *Energy Storage Mater.* 13 (2018) 168–174.
- [23] X. Dai, F. Wan, L. Zhang, H. Cao, Z. Niu, Freestanding graphene/VO₂ composite films for highly stable aqueous Zn-ion batteries with superior rate performance, *Energy Storage Mater.* 17 (2019) 143–150.
- [24] Z. Guo, Y. Ma, X. Dong, J. Huang, Y. Wang, Y. Xia, An environmentally friendly and flexible aqueous zinc battery using an organic cathode, *Angew. Chem. Int. Ed.* 57 (2018) 11737–11741.
- [25] H.Y. Shi, Y.J. Ye, K. Liu, Y. Song, X. Sun, A long cycle-life self-doped polyaniiline cathode for rechargeable aqueous zinc batteries, *Angew. Chem. Int. Ed.* 130 (2018) 16597–16601.
- [26] C. Xia, J. Guo, Y. Lei, H. Liang, C. Zhao, H.N. Alshareef, Rechargeable aqueous zinc-ion battery based on porous framework zinc pyrovanadate intercalation cathode, *Adv. Mater.* 30 (2018) 1705580.

- [27] C. Liu, Z. Neale, J. Zheng, X. Jia, J. Huang, M. Yan, M. Tian, M. Wang, J. Yang, G. Cao, Expanded hydrated vanadate for high-performance aqueous zinc-ion batteries, *Energy Environ. Sci.* 12 (2019) 2273–2285.
- [28] Z.X. Wei, D.X. Wang, X. Yang, C.Z. Wang, G. Chen, F. Du, From crystalline to amorphous: an effective avenue to engineer high-performance electrode materials for sodium-ion batteries, *Adv. Mater. Interfaces* 5 (2018) 14.
- [29] Z.S. Wu, Y. Zheng, S. Zheng, S. Wang, C. Sun, K. Parvez, T. Ikeda, X. Bao, K. Mullen, X. Feng, Stacked-layer heterostructure films of 2D thiophene nanosheets and graphene for high-rate all-solid-state pseudocapacitors with enhanced volumetric capacitance, *Adv. Mater.* 29 (2017) 1602960.
- [30] S. Zheng, W. Lei, J. Qin, Z.-S. Wu, F. Zhou, S. Wang, X. Shi, C. Sun, Y. Chen, X. Bao, All-solid-state high-energy planar asymmetric supercapacitors based on all-in-one monolithic film using boron nitride nanosheets as separator, *Energy Storage Mater.* 10 (2018) 24–31.
- [31] H. Xiao, Z.-S. Wu, F. Zhou, S. Zheng, D. Sui, Y. Chen, X. Bao, Stretchable tandem micro-supercapacitors with high voltage output and exceptional mechanical robustness, *Energy Storage Mater.* 13 (2018) 233–240.
- [32] S. Zheng, Z.-S. Wu, S. Wang, H. Xiao, F. Zhou, C. Sun, X. Bao, H.-M. Cheng, Graphene-based materials for high-voltage and high-energy asymmetric supercapacitors, *Energy Storage Mater.* 6 (2017) 70–97.
- [33] Y. Dong, Z.-S. Wu, W. Ren, H.-M. Cheng, X. Bao, Graphene: a promising 2D material for electrochemical energy storage, *Sci. Bull.* 62 (2017) 724–740.
- [34] J. Ding, Z. Du, L. Gu, B. Li, L. Wang, S. Wang, Y. Gong, S. Yang, Ultrafast Zn^{2+} intercalation and deintercalation in vanadium dioxide, *Adv. Mater.* 30 (2018) 1800762.
- [35] F. Wan, L.L. Zhang, X. Dai, X.Y. Wang, Z.Q. Niu, J. Chen, Aqueous rechargeable zinc/sodium vanadate batteries with enhanced performance from simultaneous insertion of dual carriers, *Nat. Commun.* 9 (2018) 11.
- [36] C. Xia, J. Guo, P. Li, X. Zhang, H.N. Alshareef, Highly stable aqueous zinc-ion storage using a layered calcium vanadium oxide bronze cathode, *Angew. Chem. Int. Ed.* 57 (2018) 3943–3948.
- [37] P. He, Y. Quan, X. Xu, M. Yan, W. Yang, Q. An, L. He, L. Mai, High-performance aqueous Zinc-ion battery based on layered $H_2V_3O_8$ nanowire cathode, *Small* 13 (2017) 1702551.
- [38] T. Wei, Q. Li, G. Yang, C. Wang, High-rate and durable aqueous zinc ion battery using dendritic $V_{10}O_{24}\cdot 12H_2O$ cathode material with large interlamellar spacing, *Electrochim. Acta* 287 (2018) 60–67.
- [39] V. Soundharajan, B. Sambandam, S. Kim, M.H. Alfaruqi, D.Y. Putro, J. Jo, S. Kim, V. Mathew, Y.K. Sun, J. Kim, $Na_2V_6O_{16}\cdot 3H_2O$ barnesite nanorod: an open door to display a stable and high energy for aqueous rechargeable Zn-ion batteries as cathodes, *Nano Lett.* 18 (2018) 2402–2410.
- [40] G. Li, Z. Yang, Y. Jiang, C. Jin, W. Huang, X. Ding, Y. Huang, Towards polyvalent ion batteries: a zinc-ion battery based on NASICON structured $Na_3V_2(PO_4)_3$, *Nano Energy* 25 (2016) 211–217.
- [41] M.H. Alfaruqi, V. Mathew, J. Song, S. Kim, S. Islam, D.T. Pham, J. Jo, S. Kim, J.P. Baboo, Z. Xiu, K.S. Lee, Y.K. Sun, J. Kim, Electrochemical zinc intercalation in lithium vanadium oxide: a high-capacity zinc-ion battery cathode, *Chem. Mater.* 29 (2017) 1684–1694.
- [42] T. Brezesinski, J. Wang, S.H. Tolbert, B. Dunn, Ordered mesoporous alpha- MoO_3 with iso-oriented nanocrystalline walls for thin-film pseudocapacitors, *Nat. Mater.* 9 (2010) 146–151.
- [43] T. Brezesinski, J. Wang, J. Polleux, B. Dunn, S.H. Tolbert, Templatized nanocrystal-based porous TiO_2 films for next-generation electrochemical capacitors, *J. Am. Chem. Soc.* 131 (2009) 1802–1809.
- [44] Y. Fu, Q. Wei, G. Zhang, X. Wang, J. Zhang, Y. Hu, D. Wang, L. Zuin, T. Zhou, Y. Wu, S. Sun, High-performance reversible aqueous Zn-ion battery based on porous MnO_x nanorods coated by MOF-derived N-doped carbon, *Adv. Energy Mater.* 8 (2018) 1801445.
- [45] L. Ma, N. Li, C. Long, B. Dong, D. Fang, Z. Liu, Y. Zhao, X. Li, J. Fan, S. Chen, S. Zhang, C. Zhi, Achieving both high voltage and high capacity in aqueous Zinc-ion battery for record high energy density, *Adv. Funct. Mater.* 29 (2019) 1906142.
- [46] N. Zhang, Y. Dong, M. Jia, X. Bian, Y. Wang, M. Qiu, J. Xu, Y. Liu, L. Jiao, F. Cheng, Rechargeable aqueous $Zn\text{-}V_2O_5$ battery with high energy density and long cycle life, *ACS Energy Lett.* 3 (2018) 1366–1372.
- [47] H. Pan, Y. Shao, P. Yan, Y. Cheng, K.S. Han, Z. Nie, C. Wang, J. Yang, X. Li, P. Bhattacharya, K.T. Mueller, J. Liu, Reversible aqueous zinc/manganese oxide energy storage from conversion reactions, *Nat. Energy* 1 (2016) 16039.
- [48] X.-Z. Zhai, J. Qu, S.-M. Hao, Y.-Q. Jing, W. Chang, J. Wang, W. Li, Y. Abdelkrim, H. Yuan, Z.-Z. Yu, Layered birnessite cathode with a displacement/intercalation mechanism for high-performance aqueous zinc-ion batteries, *Nano-Micro Lett.* 12 (2020) 56.
- [49] L. Shan, Y. Yang, W. Zhang, H. Chen, G. Fang, J. Zhou, S. Liang, Observation of combination displacement/intercalation reaction in aqueous zinc-ion battery, *Energy Storage Mater.* 18 (2019) 10–14.
- [50] G.Q. Sun, H.S. Yang, G.F. Zhang, J. Gao, X.T. Jin, Y. Zhao, L. Jiang, L.T. Qu, A capacity recoverable zinc-ion micro-supercapacitor, *Energy Environ. Sci.* 11 (2018) 3367–3374.
- [51] M.F. El-Kady, V. Strong, S. Dubin, R.B. Kaner, Laser scribing of high-performance and flexible graphene-based electrochemical capacitors, *Science* 335 (2012) 1326–1330.
- [52] J. Liu, C. Guan, C. Zhou, Z. Fan, Q. Ke, G. Zhang, C. Liu, J. Wang, A flexible quasi-solid-state nickel-zinc battery with high energy and power densities based on 3D electrode design, *Adv. Mater.* 28 (2016) 8732–8739.
- [53] X. Wang, S. Zheng, F. Zhou, J. Qin, X. Shi, S. Wang, C. Sun, X. Bao, Z.-S. Wu, Scalable fabrication of printed $Zn//MnO_2$ planar micro-batteries with high volumetric energy density and exceptional safety, *Natl. Sci. Rev.* 7 (2020) 64–72.
- [54] S. Yan, K.P. Abhilash, L. Tang, M. Yang, Y. Ma, Q. Xia, Q. Guo, H. Xia, Research advances of amorphous metal oxides in electrochemical energy storage and conversion, *Small* 15 (2018) 1804371.
- [55] S. Luo, L. Xie, F. Han, W. Wei, Y. Huang, H. Zhang, M. Zhu, O.G. Schmidt, L. Wang, Nanoscale parallel circuitry based on interpenetrating conductive assembly for flexible and high-power zinc ion battery, *Adv. Funct. Mater.* 29 (2019) 1901336.
- [56] Z.S. Wu, X.L. Feng, H.M. Cheng, Recent advances in graphene-based planar micro-supercapacitors for on-chip energy storage, *Natl. Sci. Rev.* 1 (2014) 277–292.